International Journal of Robotics and Automation, Vol. 36, 2021

Special Issue: Automatic Detection and Assessment of Bridge Structures

STRESS MONITORING OF THE TENSILE REINFORCEMENT IN A BRIDGE BASED ON SELF-MAGNETIC-FLUX LEAKAGE

Jun Chen,*,** Kui Tan,* Senhua Zhang,* and Siyu Zhao*

Abstract

The stress of the reinforcements of a bridge affects its safety. In this research, the stress state of internal reinforcements was studied based on the Jiles–Atherton (J–A) force magnetic coupling model and the dislocation theory. The self-magnetic-flux leakage (SMFL) monitoring method was employed to monitor the stress. After analysing the relationship between the stress and the SMFL signals, an SMFL monitoring experiment was carried out for the reinforced concrete beam. The experimental results agreed with the theory, which showed the boundary characteristics and variation characteristics of the SMFL signal curve. The SMFL signals were sensitive to the stress of the reinforcements. When the stress reached one-third of the ultimate load, a significant signal on the SMFL curve was observed. When the stress reached one-half of the ultimate load, a "smaller stress-larger stress" limit of the SMFL signals was observed. After unloading, the SMFL curve showed the characteristic signals that corresponded to the residual deformation. Thus, the stress state of the internal reinforcements could be determined according to the change in the SMFL signals. The proposed method provided a reliable basis for the subsequent evaluation of the stress state of the reinforcement, damage state, and safe operation state of the bridge.

Key Words

Reinforced concrete beam bridge, self-magnetic-flux-leakage, stress state, monitoring

1. Introduction

The operation safety of bridges is vital. The standards are updated with the increase of a bridge's bearing capacity. There are marked problems with in-service bridges. The problems include serious overloading and the phenomenon of the old design data with current specifications being inconsistent. Reinforced concrete structures are widely used in bridge engineering [1]. The bearing capacity of a concrete structure is improved by the reinforcements. However, bridge defects are inevitable, and the durability of concrete bridges is affected [2]. Additionally, the bearing capacity is affected greatly, which endangers the safety of the bridges [3]. The assessment of a bridge is important to guarantee the safety of a bridge. The stress state of the reinforcement within a bridge is an effective indicator of the evaluation of the bridge structure safety. Thus, the assessment can provide a good basis for bridge reinforcement and maintenance.

There are a variety of methods for detecting reinforcement stress. These methods can be divided into destructive testing methods and non-destructive testing methods [4]–[6]. A destructive testing method needs to damage a structure. Thus, the use of destructive testing methods is limited. Existing non-destructive testing methods include the resistance strain gauge measuring method, the fibre Bragg grating sensor method, the ultrasonic method, the X-ray method, and the self-magnetic-flux leakage (SMFL) method. The resistance strain gauge measuring method [7], [8] can measure the strain of reinforcements, but it requires the strain gauge to be pasted onto the reinforcements. For the fibre Bragg grating sensor method, sensors are embedded on reinforcements [9]–[11]. The changes in the parameters of the sensor are collected to evaluate the state of the reinforcement. The fibre Bragg grating sensor method has disadvantages such as being expensive and having poor economic benefits. For the ultrasonic method [12]–[14], the corrosion of reinforcement is analysed according to the parameter variation of an ultrasonic signal. However, the accuracy of the received signal is affected by the dispersion phenomenon. The X-ray method [15], [16] is not convenient to use in the field, and the detection depth is limited.

* College of Civil Engineering, Chongqing Jiaotong University, Chongqing 400074, P.R.China; e-mail: {20475446,120717268}@qq.com, shzhang@mails.cqjtu.edu.cn, z18375753342@163.com

** Chongqing City Transportation Development and Investment Group Co. Ltd., Chongqing 401121, P.R. China
Corresponding author: Senhua Zhang

Recommended by Dr. Jingzhou Xin
(DOI: 10.2316/J.2021.206-0538)

The SMFL method [17] is a new non-destructive testing method. This method can identify and evaluate the stress state, damage, and degree of reinforcement with the SMFL signals. The SMFL signals are collected on the surface of reinforcement under stress. This method has the advantages of high detection speed and low cost. The macroscopic defects, microscopic damage, and stress concentrations inside the components can be detected with this method.

In this research, the stress state of internal reinforcements was studied using the Jiles–Atherton (J–A) force magnetic coupling model and the dislocation theory. The theoretical background of the J–A model and the dislocation theory was analysed. An experiment was carried out to verify the theoretical analysis. According to the experimental results, the relationship between the stress state of the reinforcement and the SMFL signal was discussed. The results showed that the SMFL method could monitor the stress of the reinforcement inside the concrete with the advantages of no extra excitation, simple operation, a wide range of use, and good economic benefits.

2. Theory

The J–A model illustrates the magneto-mechanical coupling effect under a unidirectional stress. Ferromagnetic materials are composed of magnetic domains that are different in all the orientations. When there is an external force on the ferromagnetic materials, the internal magnetic domain wall experiences reversible deformation and irreversible displacement. As expressed in (1), uneven change occurs with the intensity of the magnetization within the stress concentration areas of ferromagnetic materials. The magnetizations include reversible magnetization (M_{rev}) and irreversible magnetization (M_{irr}).

$$M = M_{\mathrm{rev}} + M_{\mathrm{irr}}. \tag{1}$$

As shown in (2), the stress changes the internal effective field through the magnetostriction coefficient. The change is equal to adding an equivalent magnetic field.

$$H_\sigma = \frac{3\sigma}{2\mu_0}\left(\frac{\mathrm{d}\lambda}{\mathrm{d}M}\right)_\sigma = \frac{3\sigma_0}{2\mu_0}\left(\frac{\mathrm{d}\lambda}{\mathrm{d}M}\right)_\sigma (\cos^2\theta - \upsilon\sin^2\theta). \tag{2}$$

The relationship between magnetization and stress, expressed in (3), can be deduced from the relationship between the magnetization (M), reversible magnetization (M_{rev}), irreversible magnetization (M_{irr}), and paramagnetic magnetization (M_{an}) of magnets:

$$\frac{dM}{d\sigma} = \frac{\sigma}{\xi E}(M_{\mathrm{an}} - M) + c\frac{dM_{\mathrm{an}}}{d\sigma}. \tag{3}$$

The magnetization intensity relates to the stress and initial magnetic state of a material. According to the J–A model, the hysteresis effect is caused by the pinning effect of the domain walls. The limitation of (3) is that it can be only applied to the elastic stage [18]. The reason for this is that the relationship between magnetization and stress in the plastic phase is too complex to be described by the quantitative model. The leakage magnetic field on the surface of the stress concentration region is expressed by the normal component passing through the zero points. The tangential component shows the peak in this region. Changes in the flux leakage for each component can be monitored for further analysis.

According to the J–A model, for the same stress and external field, the influence of the small stress on the magnetization of a ferromagnet may be strengthened or weakened. Under the infliction of large stress, the variation of the magnetization relates to the stress. The SMFL signal can scarcely be observed before the stress amplitude leads to the significant development of micro defects. For most mild steel, the critical stress is about 60–80 MPa (about 0.3 times the yield strength). Additionally, periodic stress makes the magnetization of ferromagnetic materials undergo irreversible evolution, which causes the magnetization of ferromagnetic materials to be unable to recover. Equation (3) applies to the magnetoelastic phase of ferromagnetic materials. When ferromagnetic materials yield, the SMFL consists of the elastic magnetic flux leakage that satisfies the J–A model and the plastic part caused by the plastic deformation. After unloading, the elastic part is restored, while the plastic part still exists [19].

The dislocation theory describes the plastic phase of steel reinforcement. The arrangement of the metal crystals inside the reinforcement is unordered. When the reinforcement is tensed to the plastic stage, the entire row of atoms in an internal metal crystal will not slide along a slip surface. The row of atoms in the internal metal crystal will slip between the crystal surfaces according to the development trend of the defects.

3. Experiment Process

3.1 Preparation of Test Specimens

An experiment was carried out to explore the relationship between the SMFL signal and the stress of the steel bar of the reinforced concrete beam. Twelve pieces of reinforced concrete beams were prepared. The geometric size of each specimen was 100 mm × 200 mm × 1,850 mm. The compressive strength of the concrete was 40 MPa. The thickness of the protective layer was 25 mm. The stirrups were single-leg hoops. The arrangement of the longitudinal tension bars and compression bars is shown in Table 1.

The diameters of the tensioned steel bars were divided into 8 mm and 12 mm. The diameters of the compressed steel bars were 8 mm. For Groups A and C, the compressed steel bars were cut off in the bending section. The reinforcements of the specimens are shown in Fig. 1.

3.2 Experiment Method of "Four-point Bending" Loading and Unloading

As shown in Fig. 2, the "four-point bending" loading method was used to process the loading procedure. The pressure was applied by the jack and distributed with the

Table 1
Rebar Layout Information

Category	Reinforcement Method	Quantities	Numbering
A	Tensioned steel bar: 2Φ8 Compressed steel bar (cut-off): 2Φ8	3	8-D-1–8-D-3
B	Tensioned steel bar: 2Φ8 Compressed steel bar: 2Φ8	3	8-T-1–8-T-3
C	Tensioned steel bar: 2Φ12 Compressed steel bar (cut-off): 2Φ8	3	12-D-1–12-D-3
D	Tensioned steel bar: 2Φ12 Compressed steel bar: 2Φ8	3	12-T-1–12-T-3

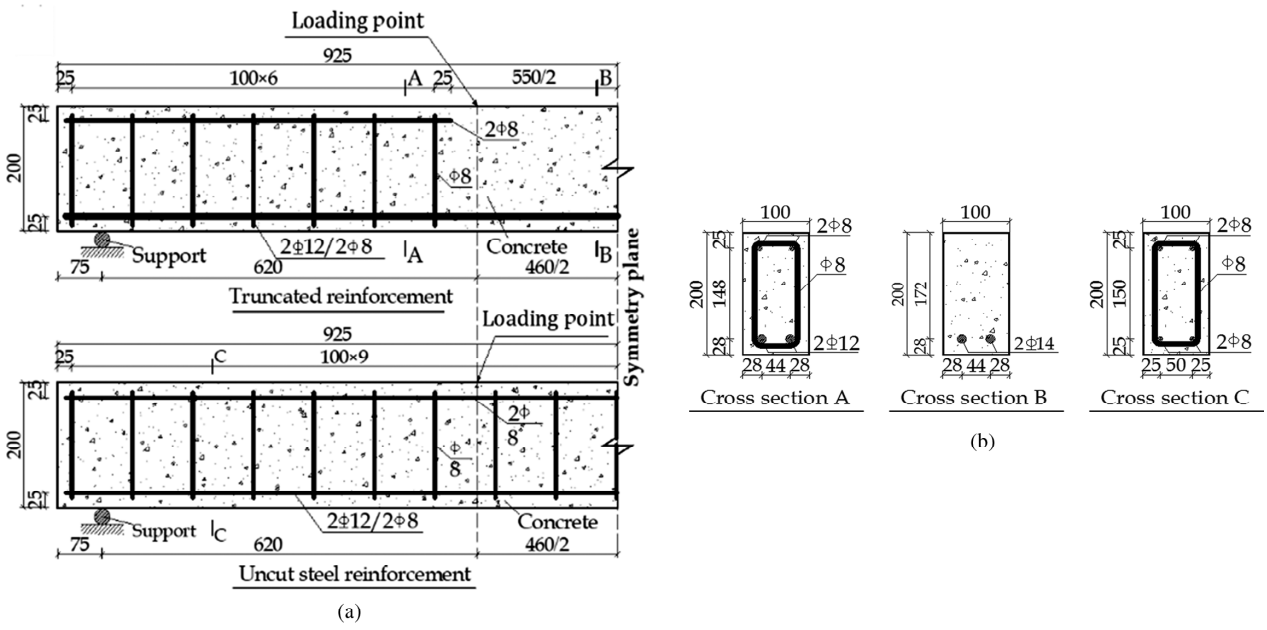

Figure 1. Reinforcement diagram of the reinforced concrete specimens: (a) front view and (b) side view (units: mm).

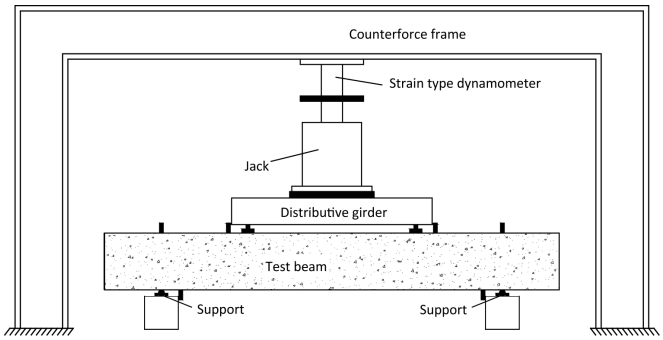

Figure 2. Four-point bending load test layout.

distributive girder. The stress was obtained with a strain gauge (297 $\mu\varepsilon$/T). The specimen was unloaded when the ultimate bearing capacity was reached. The judgement of the ultimate bearing capacity included four indicators. The indicators included the pulling of the main rib, the width of the vertical crack reaching 1.5 mm, the deflection reaching 1/50th of the span, and the crushing of the concrete in the compression zone. The loading and unloading were continuous. The SMFL signal was monitored and collected during the process.

3.3 Experiment Method of the SMFL Monitoring Method

Fixed-point monitoring was used in the experiment. As shown in Fig. 3 and Table 2, five measuring points were located on the surface of the specimen. Five sensors were fixed to the positions.

4. Experimental Results

The destruction mode of each specimen was proper steel bar damage. The ultimate bearing capacity of the specimen was determined by the yield strength of the longitudinal reinforcement. The damage indicator of each specimen was the maximum vertical crack width. In addition, the

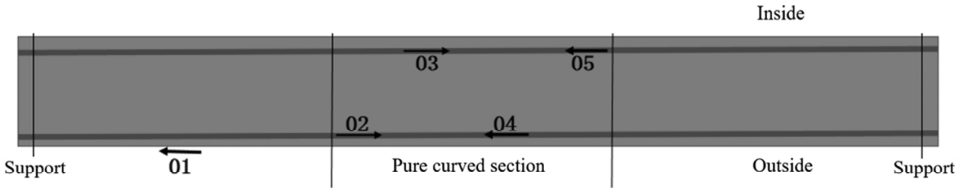

Figure 3. Measuring points of the specimens.

Table 2
Information about the Measuring Points

Measuring Point Number	Position
1	Midpoint of the left side of the curved section, above the tensioned steel bar
2	Left side of the pure curved section, below the tensioned steel bar
3	In the pure curved section, near the middle of the inner tensioned steel bar
4	In the pure curved section, near the middle of the outer tensioned steel bar
5	Right side of the pure curved section, below the tensioned steel bar

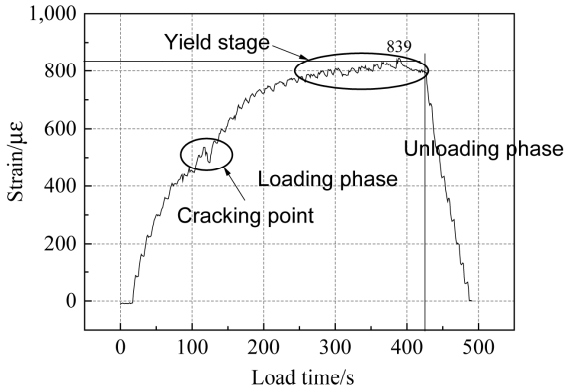

Figure 4. 8-D-1 test beam loading and unloading load (strain) curve.

strain–time curves for the same type of specimens were similar.

The results of specimen 8-D-1 were taken as an example. The ultimate strain was calculated at 0.65 m away from the loading point. The ultimate strain of the specimen was 839 $\mu\varepsilon$, and the calculated ultimate bending strength was 9.18 kN·m. The cracking points and the yield stage were observed during the loading process. The strain–time curve of the loading and unloading stages is shown in Fig. 4. The curve was jagged because the loading was manually processed and held to collect the data.

The stirrups enhanced the shear capacity. In the pure bending section, the shear force was zero. For this condition, the stirrups suppressed the bending deformation of the tensioned reinforcements and the compressed reinforcements. The ultimate strain value of specimen 8-D-1 was 800 $\mu\varepsilon$. The ultimate strain value of specimen 8-T-1 was about 1,000 $\mu\varepsilon$. This meant that the bearing capacity of the specimen in the pure bending section increased if the stirrups were contained.

In the experiment, the sensor collected SMFL signals in the X-, Y-, and Z-directions. These SMFL signals were named B_x, B_y, and B_z, respectively. As shown in Fig. 5, the SMFL curve was jagged, which indicated that the SMFL signal of the reinforcements was sensitive to the change of the stress. This indicated that the SMFL signal could be used to detect the stress state of the reinforcements.

The SMFL signals in the pure bending section of the cut specimens and the uncut specimens were compared. The absolute value of the SMFL signal in the Y-direction of the 8-D-1-Y was higher than that of the 8-T-1-Y. Because the stirrups could limit the bending of the tension reinforcement in the X–Y plane, the bending degree of the measuring point was higher than that of the specimen without the stirrups. The tensile stress of the reinforcements was also higher. Thus, the internal magnetic domain of the steel bar was more obvious in the X–Y plane, and the magnetization was relatively larger.

In the Z-direction, the value of the SMFL signal of the 8-D-1-Z corresponding point was high. However, the absolute value of the 8-D-1-Z was smaller than that of the 8-T-1-Z. Moreover, the SMFL fluctuated in some areas and the regularity was poor. This demonstrated that the stirrup could affect the SMFL signal of the tensile reinforcements in the pure bending section.

The SMFL signal of 8-D-1, 8-T-2, 12-D-2, and 12-T-1s was analysed. To diminish the influence of the stirrups, the SMFL signal in the X-direction was analysed. As shown in Fig. 6, at the beginning of the loading stage, the beam worked in the full section. The tensile stress was sustained by the concrete. Thus, the magnetization of the reinforcement was low. The reasons for this were the small tensile stress and the slight magnetic domain motion. The signals of each specimen were small and stationary, indicating that the reinforcements were in the elastic stage.

With the load increasing, plastic deformation occurred in the tension zone on the lower side of the concrete. As shown in Fig. 6, when the time was 90 s, the SMFL signal of each measuring point fluctuated. At this time, the magnetic domain inside the steel bar changed. When the load increased to 0.3–0.4 times the ultimate bearing capacity of the specimen, the SMFL signal fluctuated in

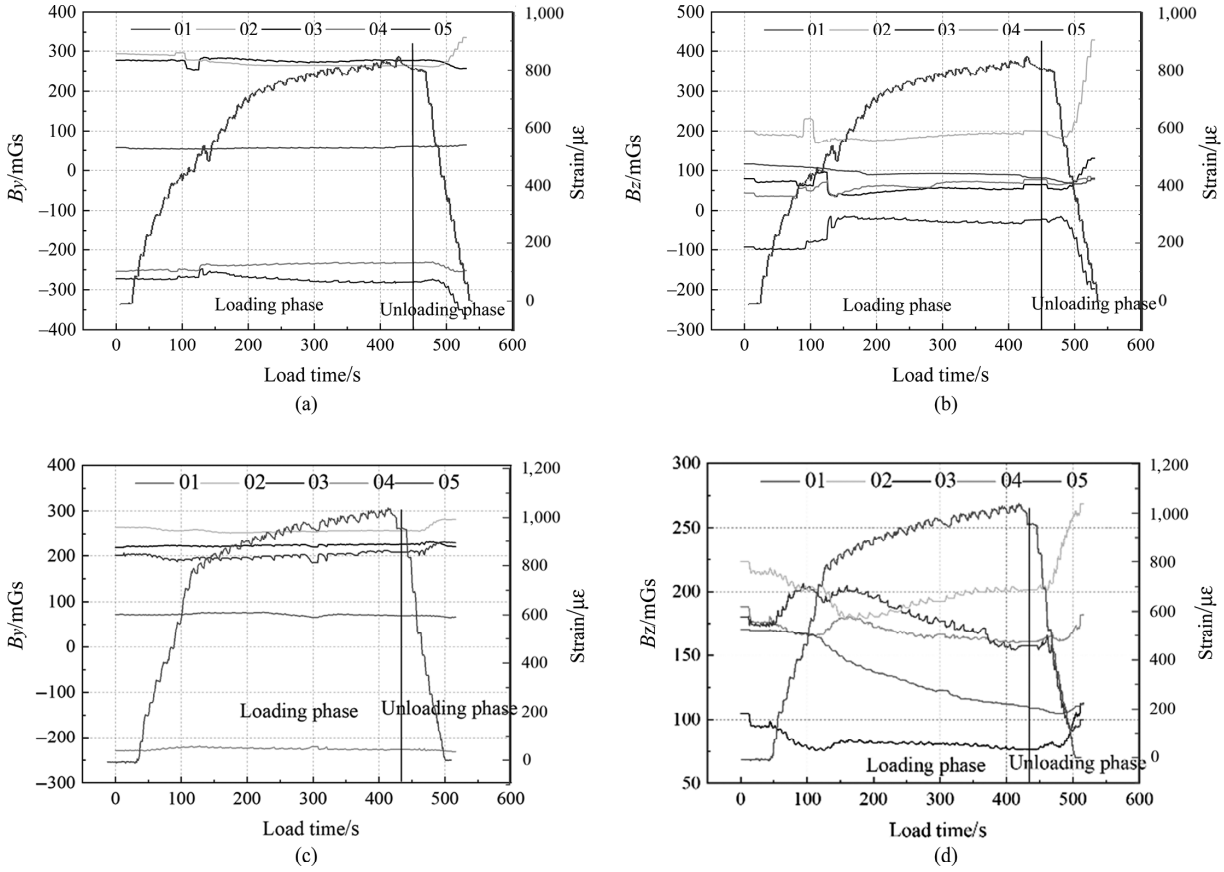

Figure 5. $Y-Z$ direction leakage magnetic signal comparison: (a) 8-D-1-Y; (b) 8-D-1-Z; (c) 8-T-1-Y; and (d) 8-T-1-Z.

a small range. Because the internal magnetic domain of the reinforcement changed, the SMFL field at the stress concentration area was generated. This demonstrated that the reinforced concrete beam had a "significant limit" of the SMFL signal. The signal appeared when the load reached about one-third of the beam's ultimate bearing load. The reinforcement was still in the elastic working state.

The first vertical crack of 8-D-1 and 8-T-2 was generated when the time was 120 s. The first vertical crack of 12-D-2 and 12-T-1 was generated when the time was 150 s. At the time, the tensile strain and the tensile stress of the concrete at the edge of the tension zone reached the maximum values. According to the bending law of the reinforced concrete beam, the tensile stress was sustained by the reinforcement once the vertical crack occurred. At the same time, there was a "smaller stress-larger stress" limit (cracking limit) for the SMFL signal of the reinforcement. The load at the boundary was about 0.5 times the ultimate load. Beyond this limit, the trend of the SMFL signal at each measuring point was stabilized.

After the concrete cracked, the tensile stress of the reinforcement increased, and the plastic deformation increased. The J–A model was no longer suitable. In the initial stage of plastic deformation, isolated dislocations were formed in the reinforcement. The isolated dislocations caused the increase of the SMFL field on the steel surface and the irreversible magnetization. Additionally, the solitary dislocations began to decrease with the increase of the plastic deformation.

As shown in Fig. 6(a), when the time was 250 s, the stress of the reinforcement was stable even though its strain increased. This meant that the reinforcement reached the yield state. In the yielding stage, the plastic deformation of the reinforcement increased. The large plastic deformation caused the dislocation entanglement of the high dislocation density inside the reinforcement to form strong pinning. Because the tensile stress could not overcome the limitation on the movement of the magnetic domain wall, the irreversible magnetization process was reduced and the rate of change of the SMFL field on the surface of the reinforcement began to decrease.

When the plastic deformation increased further, a dislocation cell structure with higher pinning energy was formed. The dislocation cell structure prevented the movement of the magnetic domain wall. The changing rate of the SMFL field on the surface of the reinforcement decreased. The SMFL field showed a horizontal stable change. After the "cracking limit" was reached, the plastic deformation of the reinforcement increased. The SMFL model gradually changed horizontally without significant fluctuation.

When the width of the crack reached 1.5 mm, the specimen reached its ultimate bearing capacity. In the unloading stage, the SMFL signal changed alternately. The changing degree of the signal was different. The SMFL

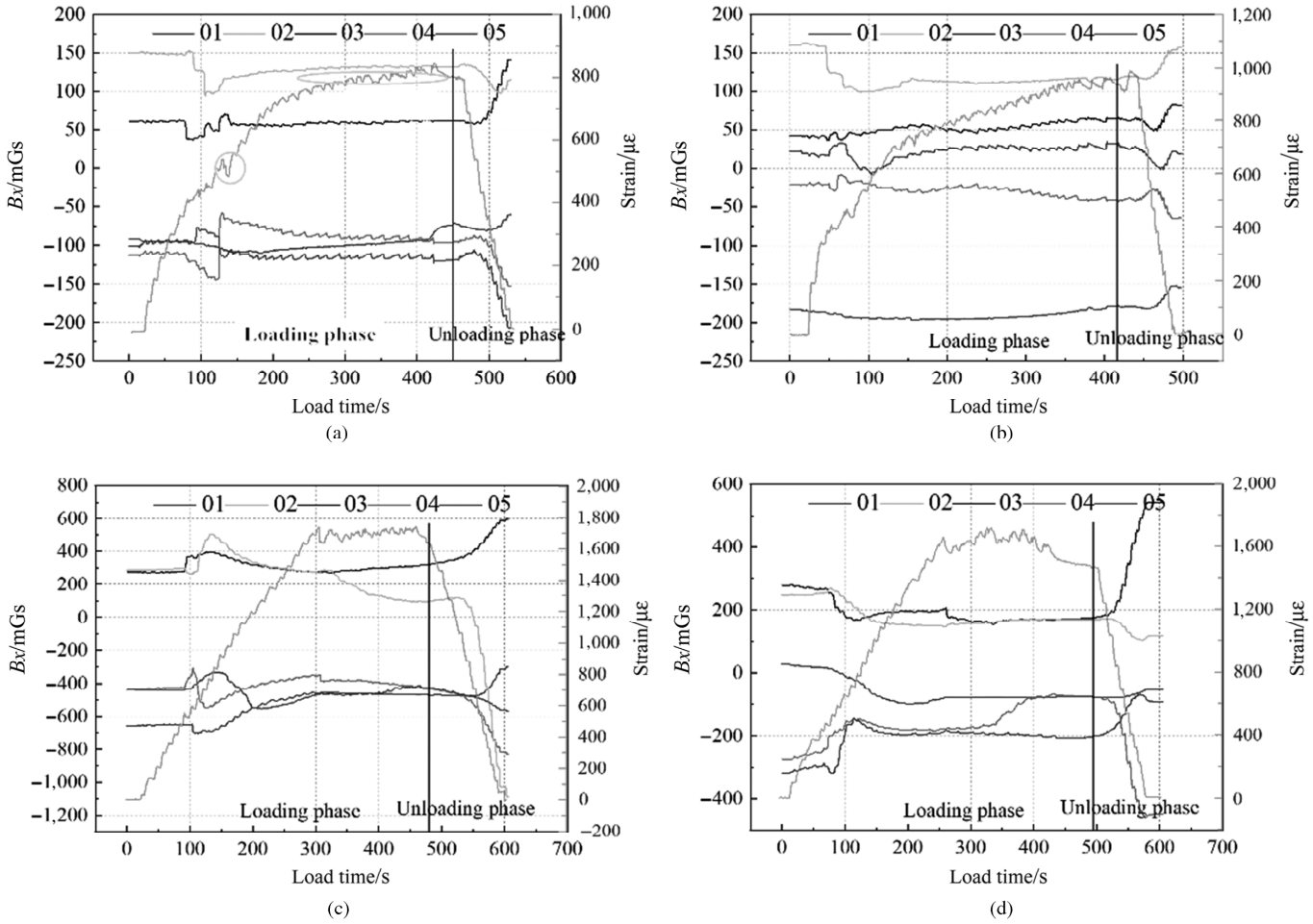

Figure 6. X-direction leakage magnetic signal comparison: (a) 8-D-1-X; (b) 8-T-2-X; (c) 12-D-2-X; and (d) 12-T-1-X.

intensity was different from that of the initial stage of loading. This was because the damage of the reinforcement maintained the yield strength. At the time, the elastic deformation recovered. However, the plastic deformation could not recover. The high-density dislocation structure was retained, which preserved the high pinning energy. The irreversible orientation of the internal magnetic domain caused the irreversible SMFL field strength of the reinforcement. Therefore, there was a certain difference between the surface magnetic field strength after the unloading of the reinforcement and the surface magnetic field strength at the initial stage of loading.

5. Conclusion

According to the above analysis, the SMFL signal of the reinforcement could reflect the stress and strain state of the reinforcement. The conclusions could be drawn as follows.

1. The SMFL signal of the reinforcement was sensitive to stress. The SMFL signal could be used as the basis of the stress and strain monitoring of the reinforcements.
2. There was a significant limit in the SMFL monitoring curve. The applied load was about 0.3–0.4 times the ultimate load of the reinforced concrete beam. For this condition, the reinforcement worked in the elastic state.
3. The SMFL monitoring curve had a crack limit that occurred when the load was 0.5 times the ultimate load. When this limit was reached, the concrete cracked. Then the stress was sustained by the reinforcement. When the SMFL signal was stabilized, the reinforcement yielded and plastic deformation occurred.
4. The SMFL signal that was collected after unloading differed from the signal that was collected before the loading, which demonstrated the existence of residual plastic deformation of the reinforcement.

Acknowledgement

This research was financially supported by the Technology Innovation and Application Demonstration Project of Chongqing (cstc2018jscx-mszdX0084).

References

[1] R. Figueira, Electrochemical sensors for monitoring the corrosion conditions of reinforced concrete structures: A review, *Applied Sciences*, *7*(11), 2017, 1157.

[2] B. Elsener, Macrocell corrosion of steel in concrete – implications for corrosion monitoring, *Cement and Concrete Composites*, *24*(1), 2002, 65–72.

[3] C.A. Apostolopoulos and V.G. Papadakis, Consequences of steel corrosion on the ductility properties of reinforcement bar, *Construction and Building Materials*, *22*(12), 2008, 2316–2324.

[4] R. Abe, H. Takemoto, T. Suzuki, *et al.*, Basic study on low-temperature cracking of asphalt pavement using stress release method, *Journal of Pavement Engineering, JSCE*, *9*(12), 2004, 209–217.
[5] W.J. Yi and H. Xiang, Test and analysis of working stress of reinforced concrete compression members, *Industrial Construction*, *37*(1), 2007, 52–56.
[6] H.L. Pang and S.R. Pukas, Residual stress measurements in a cruciform welded joint using hole drilling and strain gauges, *Strain*, *25*(1), 1989, 7–14.
[7] Z. Wang, W.B. Xie, Z.H. Wang, and Y. Cao, Strain method for synchronous dynamic measurement of elastic, shear modulus and Poisson's ratio of wood and wood composites, *Construction and Building Materials*, *182*(2018), 2018, 608–619.
[8] C.H. Tan, Y.G. Shee, B.K. Yap, and F.R. Mahamd Adikan, Fiber Bragg grating based sensing system: Early corrosion detection for structural health monitoring, *Sensors and Actuators A: Physical*, *246*(2017), 2016, 123–128.
[9] C. Leung, K. Wan, and L.Q. Chen, A novel optical fiber sensor for steel corrosion in concrete structures, *Sensors*, *8*(3), 2008, 1960–1976.
[10] W.J. Li, S.C. Ho, and G.B. Song, Corrosion detection of steel reinforce concrete using combined carbon fiber and fiber Bragg grating active thermal probe, *Smart Materials and Structures*, *25*(4), 2016, 045017.
[11] A. Sharma, S. Sharma, S. Sharma, and A. Mukherjee, Ultrasonic guided waves for monitoring corrosion of FRP wrapped concrete structures, *Construction and Building Materials*, *96*(2015), 2015, 690–702.
[12] A. Michel, B.J. Pease, M.R. Geiker, and H. Stang, Monitoring reinforcement corrosion and corrosion-induced cracking using non-destructive X-ray attenuation measurements, *Cement and Concrete Research*, *41*(11), 2011, 1085–1094.
[13] P.A. Itty, M. Serdar, C.M. Akgul, and D. Parkinson, In situ 3D monitoring of corrosion on carbon steel and ferritic stainless steel embedded in cement paste, *Corrosion Science*, *83*(2014), 2014, 409–418.
[14] K. Yao, Z.D. Wang, B. Deng, and K. Shen, Experimental research on metal magnetic memory method, *Experimental Mechanics*, *52*(3), 2012, 305–314.
[15] P.P. Shi, K. Jin, P.C. Zhang, *et al.*, Quantitative inversion of stress and crack in ferromagnetic materials based on metal magnetic memory method, *IEEE Transactions on Magnetics*, *54*(10), 2018, 1–11.
[16] D.C. Jiles and L. Li, A new approach to modeling the magnetomechanical effect, *Journal of Applied Physics*, *95*(11), 2004, 7058–7060.
[17] D.C. Jiles, Theory of the magnetomechanical effect, *Journal of Physics D Applied Physics*, *28*(8), 1995, 1265–1281.
[18] C.Y. Pang, J.T. Zhou, R.Q. Zhao, *et al.*, Research on internal force detection method of steel bar in elastic and yielding stage based on metal magnetic memory, *Materials*, *12*(7), 2019, 1167.
[19] S.H. Zhang, J.T. Zhou, Y. Zhou, *et al.*, Cable tension monitoring based on the elasto-magnetic effect and the self-induction phenomenon, *Materials*, *12*(14), 2019, 2230.

Biographies

Jun Chen received his master's degree. He is now pursuing for a doctorate in Chongqing Jiaotong University, Chongqing, China. He is mainly engaged in the fields of bridge strengthening and health monitoring.

Kui Tan is pursuing his master's degree in Chongqing Jiaotong University, Chongqing, China. He is mainly engaged in the field of bridge testing and reinforcement.

Senhua Zhang is studying for a doctorate in Chongqing Jiaotong University, Chongqing, China. His research interests include bridge strengthening, construction materials and health monitoring.

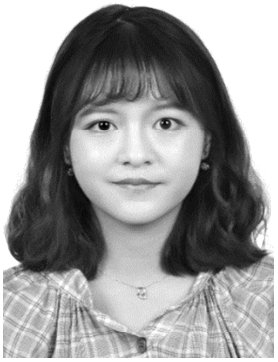

Siyu Zhao received her bachelor's degree in Chongqing Jiaotong University. She is now studying for a master's degree at Chongqing Jiaotong University. Her current research includes the inspection of corroded reinforced concrete and self-magnetic flux leakage.